MODIS Multi-Angle Implementation of Atmospheric Correct (MAIAC) Data User's Guide

Collection 6.1

Version 3.1

Principal Investigator: Alexei Lyapustin

Correspondence e-mail address:
Yujie.Wang@nasa.gov; Alexei.I.Lyapustin@nasa.gov;

Prepared by Alexei Lyapustin and Yujie Wang

Published: November, 2022

TABLE OF CONTENTS

1. Introduction ……..... 3
2. Changes in MAIAC Collection 6.1 vs C6 …… 3
3. Overview of MAIAC products 5
3.1 Tiled File Structure and Naming Convention 5
3.2 MAIAC Products: General Description 6
3.2.1 Atmospheric Properties File (MCD19A2)..... 6
3.2.2 Surface Reflectance File (MCD19A1) 7
3.2.3 Surface Gap-Filled (BRDF/NDVI/Snow Properties) File (MCD19A3) …….10
4. QA-related Comments (please read) ……..... 10
4.1 Use of Adjacency Mask 10
4.2 Selecting Best Quality BRF and AOD 11
5. MAIAC Data Specification ……..… 11
5.1. Surface Reflectance (MCD19A1) 11
5.2 Status QA definition for MCD19A1 (16-bit unsigned integer) ……..…… 12
5.3 Aerosol Optical Depth (MCD19A2) …..……. 13
5.4 AOD QA definition for MCD19A2 (16-bit unsigned integer) …… 14
5.5 Gap-Filled Surface Properties (BRDF/NDVI/Snow Properties) file (MCD19A3) ……. 15
5.6 Daily 0.05° global surface BRF CMG for Land Bands (MCD19A1CMGL) ……..… 15
5.7 Daily 0.05° global surface BRF CMG for Ocean Bands (MCD19A1CMGO) ……...… 16
5.8 Daily 0.05° global surface BRF CMG QA definition ……. 16
5.9 Daily 0.05° global AOD CMG (MCD19A2CMG) ……..….... 17
5.10 Daily 0.05° global Vegetation Index CMG (MCD19A3CMG) …… 17
6. Caveats and Known Problems ……..… 18
7. MAIAC Validation Status …… 18
8. Data ordering (browsing) ……..… 19
9. References 16
10. How to Reconstruct AOD Image From Compact AOD Records…….23
11. Compositing BRF Selection Strategy ……. 24

1. Introduction

MAIAC is an advanced algorithm which uses time series analysis and a combination of pixel- and image-based processing to improve accuracy of cloud detection, aerosol retrievals and atmospheric correction (*Lyapustin et al*., 2018; 2011a,b; 2012; publication on MAIAC C6.1 is under preparation). The underlying physical idea behind MAIAC is simple: because surface changes slowly in time compared to aerosols and clouds given the daily rate of global MODIS observations, we focus on extensive characterization of the surface background in order to improve all stages of MAIAC processing. MAIAC starts with gridding MODIS measurements (L1B data) to a fixed grid at 1km resolution in order to observe the same grid cell over time and work with polar-orbiting observations as if they were "geostationary". In this regard, this approach is fundamentally different from the conventional swath-based processing where the footprint changes with orbit and view geometry (scan angle) making it difficult to characterize the surface background.

To enable the time series analysis, MAIAC implements the sliding window technique by storing from 4 (at poles) to 16 (at equator) days of past observations in operational memory. This helps us retrieve surface BRDF from accumulated multi-angle set of observations, and detect seasonal (slow) and rapid surface change. A detailed knowledge of the previous surface state also helps MAIAC's internal dynamic land-water-snow classification including snow detection and characterization.

Consistently with the entire C6.1 MODIS land processing, the top-of-atmosphere (TOA) L1B reflectance includes standard C6.1 calibration (*Toller et al*., 2014; *Xiong et al*., 2020) augmented with polarization correction for MODIS Terra (*Meister et al*., 2012), residual de-trending and MODIS Terra-to-Aqua cross-calibration (*Lyapustin et.al*, 2014). The L1B data are first gridded into 1km MODIS sinusoid grid using area-weighted method (*Wolfe et al*., 1998). Due to cross-calibration, MAIAC processes MODIS Terra and Aqua jointly as a single sensor.

MAIAC provides an inter-disciplinary suite of the atmospheric and land surface products united by the high quality cloud/snow detection and consistently derived from the MODIS observations thus observing the energy conservation principle. The MAIAC atmospheric products include AOD, column water vapor and smoke injection height at 1km resolution. Over the ocean, MAIAC retrieves AOD and fine mode fraction and reports the water-leaving reflectance. The land surface product suite includes surface reflectance (bidirectional reflectance factor, BRF) at 0.5km (MODIS bands 1-7) and at 1km (bands 1-12). It also includes several gap-filled products: 250m BRF normalized to nadir view and sun zenith angle at local 1:30pm time (equivalent of NBAR) (bands 1-2), RTLS BRDF model parameters at 1km (bands 1-8) and NDVI (1km). When snow is detected, MAIAC reports the gap-filled snow fraction and snow grain size at 1km resolution.

In C6.1, MAIAC product suite is also available at the Climate Modeling Grid (CMG) 0.05° resolution for convenience of the global analysis and modeling applications.

2. Changes in MAIAC Collection 6.1 vs C6

In MAIAC C6.1, we corrected many known deficiencies of MAIAC C6 and added new products:

Aerosol Optical Depth (AOD)

- C6 underestimated AOD at high AOD>0.6 for the biomass burning aerosols. In C6.1, we updated MAIAC regional aerosol models based on analysis of AERONET database. The C6.1 aerosol models introduced a dynamically increasing aerosol absorption at higher AOD along with decreasing effective particle size which led to a significant improvement of AOD retrieval accuracy at high AOD.
- C6 underestimated AOD in Western Sahara. In C6.1, we added an additional Western Sahara region with more absorbing mineral dust aerosol model, which improves AOD performance.
- At high AOD, the C6 sometimes showed a boundary ("jump" in AOD) between the regions with different aerosol absorption in MAIAC regional aerosol models. In C6.1, we added a 300km transitional zone where the aerosol model linearly changes from Region 1 to Region 2. This is a temporary solution which removes the AOD discontinuity on the border between different regions though may introduce weak spatial gradients across the boundary.
- The C6.1 improved the overall performance (AOD, FMF, water-leaving reflectance) over the coastal and remote ocean, including sediment-rich waters with high Red-NIR reflectance.
- MAIAC C6.1 increased maximum AOD at 0.47μm to 6 (from 4 in C6).

Smoke Plume Injection Height (PIH)

- MAIAC C6.1 introduced GDAS temperature profiles to derive PIH while the C6 algorithm used a fixed lapse rate. A preliminary assessment shows that this change improves the PIH accuracy globally.

MAIAC BRDF

- The C6 MAIAC BRDF product (MCD19A3) was reported once every 8 days. Despite MAIAC retrieves BRDF continuously with every orbit, this limitation was imposed by MODAPS to limit the output size. In C6.1, the BRDF product is reported daily.
- In MAIAC C6, MODIS calibration uncertainties in B8 (412nm) sometimes resulted in striping of AOD and SR, in particular at high VZA. As a result, the BRDF model at 412nm would display striping as well. In MAIAC C6.1, we augmented MODIS calibration in bands B3, B8 which reduced the striping at high latitudes (above 60°) but did not cancel it entirely. For this reason, MAIAC 6.1 does not retrieve BRDF parameters in band 8 still prone to calibration artifacts. Instead, the reported B8 BRDF is obtained from the Blue band (B3) by scaling it using the near-nadir ratio of the SR_{B8}/SR_{B3}. Such approach is valid due to the BRDF shape similarity in the Blue-Deep Blue spectral region where the surface reflectance is generally low.

Gap-Filled 1km Products:

NDVI and Snow Fraction (SF)/Snow Grain Size (SGS)

- MAIAC C6 reported SF and SGS per orbit for cloud-free pixels with detected snow. By the users request, MAIAC C6.1 reports daily gap-filled SF and SGS layers (file MCD19A3). In MAIAC, the gap filling is a natural process: the (SF, SGS) combination remains in MAIAC's memory for each 1km grid cell until updated with the latest cloud-free observations. Reporting (SF, SGS) once a day also reduces the total product size. The gap-

filled MAIAC NDVI is new compared to C6: it is produced at 1km resolution in a similar way and reported daily. For user's convenience, we also report the Update_Day, which gives the number of days since the last update.

Gap-Filled 250m NBAR

- The C6 MAIAC did not report the atmospherically corrected surface reflectance at 250m (was not accommodated by MODAPS). MAIAC C6.1 performs atmospheric correction of the 250m MODIS bands and reports a daily naturally gap-filled 250m nadir BRDF-adjusted (surface) reflectance (NBAR) in the Red and NIR bands. Reporting the 250m surface reflectance products once a day reduces the output size.

Climate Modeling Grid (CMG) Products (0.05° resolution)

The novel MAIAC CMG dataset includes:

- surface reflectance (bidirectional reflectance factor, BRF) in land and ocean bands 1-12 along with BRF_n (BRF normalized to a fixed geometry of SZA=45° and nadir view) and NBAR (BRF normalized to the nadir view and local sun angle at 1:30pm) – Tables 5.6-5.7;
- AOD at 0.47 μm and 0.55μm, column water vapor for MODIS Terra and MODIS Aqua, and daily average cloud fraction – Table 5.9;
- Daily NDVI, EVI and geometry-normalized $NDVI_n$, EVI_n (SZA=45° and nadir view); gap-filled NDVI – Table 5.10.

All these changes and new developments will be reported in near future (in preparation).

3. Overview of MAIAC products

MAIAC provides a suite of atmospheric and surface products in three HDF4 files (all *daily*): MCD19A1 (spectral BRF, or surface reflectance), MCD19A2 (atmospheric properties), and MCD19A3 (Gap-Filled Suite including spectral BRDF/NDVI/Snow Properties).

3.1 Tiled File Structure and Naming Convention

Products are reported on 1km sinusoidal grid. The sinusoidal projection is not optimal due to distortions at high latitudes and off the grid-center, but it is a tradeoff made by the MODIS land team for the global data processing. The gridded data are divided into 1200x1200km^2 standard MODIS tiles shown in Figure 1.

The current dataset presents data per orbit (we do not provide a daily composite image as in standard MODIS surface reflectance product MOD09). Each daily file name follows standard MODIS name convention, for instance:

MCD19A1.DayOfObservation.TileNumber.Collection.TimeOfCreation.hdf.

DayOfObservation has the format "YYYYDDD", where YYYY is year, DDD is Julian day.

TileNumber has the standard format, e.g. h11v05 for the east coast USA.

Each daily file (MCD19A1 and A2) usually contains multiple orbit overpasses (1-2 at equator and up to 30 in polar regions for combined Terra and Aqua) which represents the third (time) dimension of MAIAC daily files. The orbit number and the overpass time of each orbit are saved in global attributes "*Orbit_amount*" and "*Orbit_time_stamp*" sequentially. The Orbit_time_stamp is in the format of "YYYYDDDHHMM[TA]", where YYYY is year, DDD is Julian day, HH is hour MM is minute, T stands for Terra and A stands for Aqua. At high latitudes, only first 16 orbits with largest coverage are selected for processing per day in order to limit the file size.

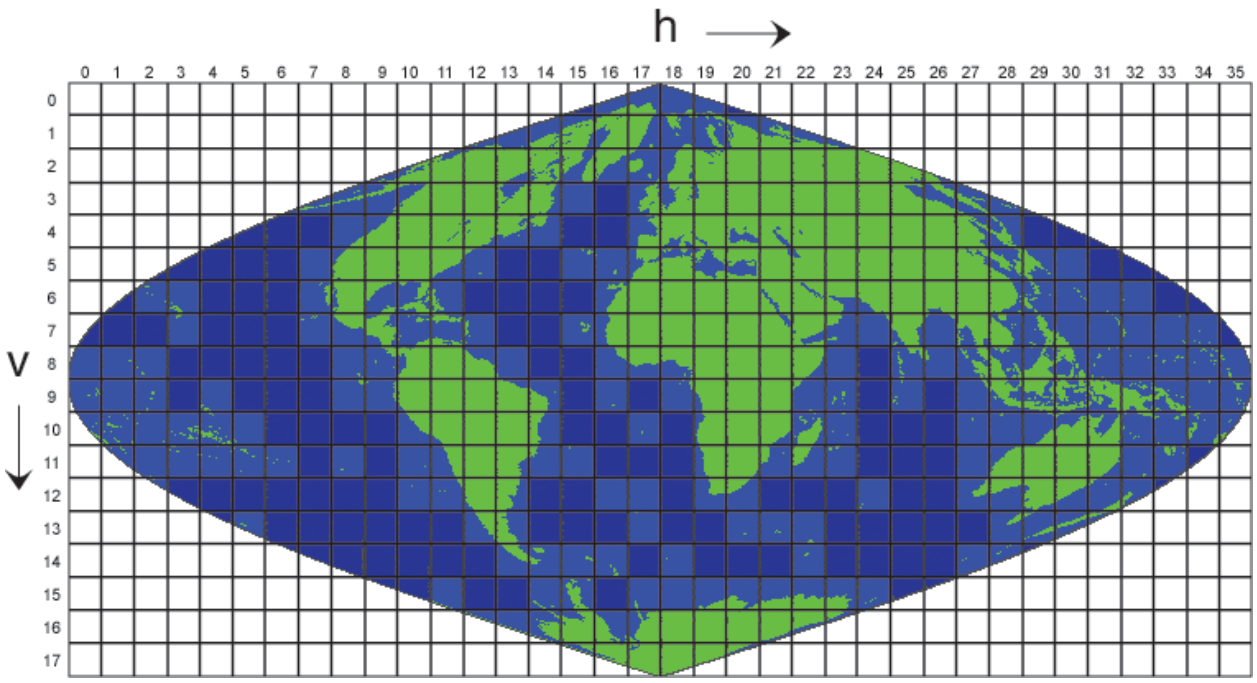

Figure 1. Illustration of MODIS Sinusoidal Tiles.

3.2 MAIAC Products: General Description

MAIAC processing is limited to global land tiles and land-containing ocean tiles (green and light blue colors in Fig. 1).

Over inland, coastal and open ocean waters, MAIAC reports AOD, fine mode fraction, and spectral reflectance of underlight (water-leaving reflectance).

3.2.1 Atmospheric Properties File (MCD19A2)

For each orbit, MAIAC *daily* MCD19A2 (atmospheric properties) file includes:

Over land:

- *column water vapor* (CWV) retrieved from MODIS near-IR bands B17-B19 at 0.94μm (in cm). CWV is reported for both clear and cloudy pixels. In the latter case, it represents water vapor above the cloud;

- *aerosol optical depth and type* (background, biomass burning or dust). The AOD is originally retrieved (and reported) in MODIS Blue band B3 (0.47μm). Because the common input for the chemical transport models and GCMs as well as AOD validation and AOD product intercomparison are standardized to 0.55μm, we also provide the "Green" band (B4) AOD. It is computed from 0.47μm based on spectral properties of regional aerosol model used in retrievals. Validation shows that quality of AOD at 0.55μm is generally close though slightly worse than the original retrieval at 0.47μm. Currently, AOD is not retrieved at high altitudes >4.2km, except when Smoke/Dust aerosol is detected. Rather, we report static "climatology" value of 0.02 which is used for atmospheric correction. Our study showed that in conditions of very low AOD, non-flat terrain and generally bright surface, MAIAC aerosol retrievals at high altitudes are unreliable.
- *AOD uncertainty:* This parameter is evaluated based on the Blue-band B3 surface brightness (reflectance) only, and thus gives only a general indication of possible increase of error over brighter surfaces;
- *Injection Height* of Smoke plume (in m above ground): Reported near detected fire hot spots when smoke plume is optically thick and exhibits brightness temperature contrast with unobscured neighbor land surface. A validation against MISR MINX and CALLIPSO CALIOP plume heights for the North America fires of 2000-2008 showed a good accuracy within ~500m (*Lyapustin et al*., 2020).

Over water:

- *AOD* outside of glint area (glint angle ≥ 40°). When MAIAC detects dust, AOD is also reported for smaller glint angles if the retrieved value is above zero.
- *Fine Mode Fraction (FMF)* is reported along with AOD over open ocean and large in-land lakes (like Great Lakes of North America). It is not retrieved over small in-land water bodies.

View Geometry over land and water *at 5km*:

- *Cosines of Solar and View zenith angles, relative azimuth, scattering angle and glint angle*.

3.2.2 Surface Reflectance File (MCD19A1)

For each orbit, MAIAC *daily* MCD19A1 (surface reflectance) file includes:

Over land (for solar zenith angles below 80°):

- *1km BRF (surface reflectance)* in MODIS land and unsaturated ocean bands B1-B12. It is produced in cloud-free and clear-to-moderately turbid ($AOD_{0.47}$<1.5) conditions;
- *500m BRF,* nested in 1km grid, in MODIS land bands B1-B7;
- *1km BRF uncertainty (Sigma_BRFn)* in MODIS Red (B1) and NIR (B2) bands. BRF uncertainty is required for higher level land algorithms, such as LAI/FPAR (*Chen, Knyazikhin et al.*, 2017), global model assimilation etc. We define it as a standard deviation of the geometrically normalized BRFn over 16-day period under assumption

that surface is stable or changes linearly in time. As such, this is the most conservative estimate of uncertainty which includes contribution from gridding, undetected clouds, errors of atmospheric correction including those from aerosol retrievals, and of surface change when reflectance change is non-linear over time. As one can see, this definition of uncertainty is much broader than the one that may come from "theoretical" considerations, but it is also much more realistic. Sigma_BRFn in the Red band can serve as a proxy of uncertainty at shorter wavelengths, where the surface is generally darker, and the NIR value can be a proxy for the longer wavelengths with high surface reflectance.

View Geometry and Kernels of RTLS BRDF model *at 5km*:

- *Cosines of Solar and View zenith angles, relative azimuth, Sun azimuth (SAZ), sensor view azimuth (VAZ), scattering angle and glint angle.*
- *Volumetric* (F_v) *and geometric-optics* (F_G) *kernels of RTLS model* for the observation geometry. Kernels are provided for geometric- (or BRDF-) normalization of spectral BRFs, which is needed in many tasks, such as change detection, geophysical and calibration trend analysis (e.g., *Lyapustin et al*., 2012; 2014) etc. Then, the BRDF (or geometry)-normalization can be done using spectral BRDF kernel weights $\{k_L, k_V, k_G\}$ from file MCD19A3 based on the following formula (see Eqs. (6) and (8) from *Lyapustin et al*., 2012):

$$BRF_n = BRF * (k_L - 0.0458621*k_V - 1.1068192*k_G)/(k_L + F_V*k_V + F_G*k_G).$$

This equation normalizes BRF from a given view geometry to the fixed geometry of nadir view and 45° sun zenith angle ($F_{0V}(45)$=-0.0458621, $F_{0G}(45)$=-1.1068192). One can easily modify normalization to a preferable Sun angle according to latitude or season, by replacing coefficients in the numerator with values from the following table 1 built for different solar zenith angles and nadir view.

The 5km reporting scale for geometry and volumetric and geometric-optics kernels is sufficient as geometry changes slowly.

SZA	F_0v(SZA)	F_{0G}(SZA)
0	0	0
1	-0.0000589	-0.0222231
2	-0.0002322	-0.0444532
3	-0.0005146	-0.0666974
4	-0.000901	-0.0889604
5	-0.0013863	-0.1112519
6	-0.0019654	-0.1335773
7	-0.0026334	-0.1559435
8	-0.0033854	-0.1783573
9	-0.0042163	-0.2008253
10	-0.0051215	-0.2233558
11	-0.006096	-0.2459545
12	-0.0071349	-0.2686286

13	-0.0082336	-0.2913864
14	-0.0093873	-0.3142342
15	-0.0105912	-0.3371795
16	-0.0118406	-0.3602294
17	-0.0131308	-0.3833919
18	-0.0144569	-0.4066738
19	-0.0158144	-0.4300835
20	-0.0171985	-0.4536282
21	-0.0186043	-0.4773155
22	-0.0200272	-0.5011534
23	-0.0214623	-0.5251498
24	-0.0229049	-0.5493125
25	-0.0243501	-0.5736493
26	-0.025793	-0.5981684
27	-0.0272287	-0.6228774
28	-0.0286523	-0.6477844
29	-0.0300587	-0.6728968
30	-0.0314429	-0.6982225
31	-0.0327997	-0.7237687
32	-0.0341241	-0.7495425
33	-0.0354105	-0.7755507
34	-0.036654	-0.8017994
35	-0.0378488	-0.8282937
36	-0.0389896	-0.8550386
37	-0.0400707	-0.8820373
38	-0.0410865	-0.9092915
39	-0.042031	-0.9368016
40	-0.0428984	-0.964565
41	-0.0436827	-0.9925762
42	-0.0443776	-1.0208257
43	-0.0449768	-1.0492985
44	-0.0454738	-1.0779734
45	-0.0458621	-1.1068192
46	-0.0461346	-1.1357927
47	-0.0462846	-1.1648338
48	-0.0463049	-1.1938568
49	-0.0461881	-1.2227401
50	-0.0459265	-1.2513024
51	-0.0455125	-1.2792587
52	-0.044938	-1.3061037
53	-0.0441948	-1.3305788
54	-0.0432743	-1.3506508

55	-0.0421677	-1.3717234
56	-0.040866	-1.3941458
57	-0.0393597	-1.4180392
58	-0.0376392	-1.44354
59	-0.0356944	-1.4708021
60	-0.033515	-1.5

Table 1. Values of V and G kernels for different SZA and nadir view (VZA=0).

3.2.3 Surface Gap-Filled BRDF/NDVI/Snow Properties File (MCD19A3)

The *daily* MCD19A3 gap-filled file includes:

- *Three parameters of RTLS BRDF model* k_{iso}, k_V, k_G (here $k_{iso} = k_L$) in MODIS bands B1-B8 at *1km*. The retrievals represent cloud-free and low aerosol ($AOD_{0.47}<0.6$) conditions.

When snow is detected, we also compute snow grain size (diameter, in mm) which governs spectral snow albedo for pure snow, and sub-pixel snow fraction. The algorithm is based on a linear mixture model of spectral snow reflectance (*Lyapustin et al.*, 2010) and pure land spectral BRDF for every land grid cell. Processing uses minimization of MODIS reflectance in bands B1, B5, B7. The residual between the best fit and MODIS observations in B1,B5,B7 is reported in parameter Snow_Fit:

- *Snow grain size* (diameter, in mm) at 1km;
- *Sub-pixel snow fraction* (range 0-1.2) at 1km;
- *Snow Fit* (rmse for the best fit and MODIS observations in B1,B5,B7) at 1km.

Over snow-free land, MAIAC C6.1 also reports:

- *NDVI at 1km*
- *250m NBAR in B1 (Red) and B2 (NIR)*. The 250m grid is nested in MAIAC 500m and 1km grid.

The BRDF-normalization of 250m NBAR uses a 1km MAIAC RTLS BRDF model.

In MAIAC, the gap filling is a natural process: the parameter (e.g., NDVI) remains in MAIAC's memory for each 1km grid cell until updated with the latest cloud-free observations. For user's convenience, we also report the Update_Day, which gives the number of days since the last update.

4. QA-related Comments (please read)

In *daily* output files, the QA bit contains cloud mask, adjacency mask, aerosol type, surface type (the result of MAIAC dynamic Land-Water-Snow classification), and a surface change mask.

4.1 Use of Adjacency Mask:

This mask gives information about detected neighbor clouds or snow (in the 3x3 pixel box). For general applications, we recommend to only use data with QA.AdjacencyMask=Normal. The value AdjacentToASingle CloudyPixel can also be used as it often represents false cloud detection. The other categories of AdjacencyMask are not recommended when using AOD. In land analysis, we do not recommend using the values SurroundedByMoreThan4CloudyPixels. The value AdjacentToCloud should be investigated for a particular application.

4.2 Selecting Best Quality BRF and AOD

To select best quality BRF, one should apply the following QA filter:

QA.AODLevel=low (0), QA.AdjacencyMask=Clear, and QA.AlgorithmInitializeStatus= initialized (0).

The best quality AOD is represented by the QA bit 0000 "Best quality". It is a combination of the two filters:

QA.CloudMask = Clear and QA.AdjacencyMask=Clear.

5. MAIAC Data Specification

Except three reported parameters (column water vapor (cm), injection height (m above ground) and snow grain size (mm)), all other reported MAIAC products are unitless.

The valid range in the MAIAC output products are given in the specification Tables below.

5.1. Surface Reflectance (MCD19A1)

SDS name	Data Type	Scale	Fill Value	Valid Range	Description
Sur_refl[1-12]	INT16	0.0001	-28672	-100 – 16000	Surface reflectance at 1km for bands 1-12
Sigma_BRFn[1-2]	INT16	0.0001	-28672	-100 – 16000	BRFn uncertainty over time at 1km, for bands 1-2
Status_QA	UINT16	n/a	0	1 – 65535	QA bits
Sur_refl_500m [1-7]	INT16	0.0001	-28672	-100 – 16000	Surface reflectance at 500m for band 1-7
cosSZA	INT16	0.0001	-28672	0 – 10000	Cosine of Solar zenith angle (5km)
cosVZA	INT16	0.0001	-28672	0 – 10000	Cosine View zenith angle (5km)
RelAZ	INT16	0.01	-28672	-18000 – 18000	Relative azimuth angle (5km)
Scattering_Angle	INT16	0.01	-28672	-18000 – 18000	Scattering Angle (5km)
SAZ	INT16	0.01	-28672	-18000 – 18000	Solar Azimuth Angle (5km)
VAZ	INT16	0.01	-28672	-18000 – 18000	View Azimuth Angle (5km)
Glint_Angle	INT16	0.01	-28672	-18000 – 18000	Glint Angle (5km)
Fv	FLOAT32	n/a	-99999	-100 – 100	RTLS volumetric kernel (5km)
Fg	FLOAT32	n/a	-99999	-100 - 100	RTLS geometric kernel (5km)

5.2 Status QA definition for MCD19A1 (16-bit unsigned integer)

Bits	Definition
0-2	**Cloud Mask** 000 --- Undefined 001--- Clear 010 --- Possibly Cloudy (detected by AOD filter) 011 --- Cloudy (detected by cloud mask algorithm) 101 --- Cloud Shadow 110 --- Fire hot spot (over land) 111 --- Water Sediments (over water)
3-4	**Land Water Snow/Ice Mask** 00 --- Land 01 --- Water 10--- Snow 11 --- Ice
5-7	**Adjacency Mask** 000 --- Normal condition/Clear 001 --- Adjacent to clouds 010 --- Surrounded by more than 4 cloudy pixels 011 --- Adjacent to a single cloudy pixel 100 --- Adjacent to snow 101 --- Snow was previously detected for this pixel
8	**AOD level** 0 --- AOD is low (<=0.6) 1 --- AOD is high (> 0.6) or undefined
9-10	**AOD Type** 00 --- Background aerosol 01 --- Smoke 10 --- Dust
11	**BRF retrieved over snow assuming AOD = 0.05** 0 --- no 1 --- yes
12	**Altitude >4.2km (land)/3.5km (water), BRF is retrieved using climatology AOD =0.02** 0 --- no 1 --- yes
13-15	**Surface Change Mask** 000 --- No change 001 --- Regular change Green up 010 --- Big change Green up 011 --- Regular change Senescence 100 --- Big change Senescence **Regular Change**: Relative change in Red and NIR nadir-normalized BRF is more than 5% but less than 15% **Big Change :** Relative change in Red and NIR nadir-normalized BRF is more than 15%

5.3 Aerosol Optical Depth (MCD19A2)

SDS name	Data Type	Scale	Fill Value	Valid Range	Description
Optical_Depth_047	INT16	0.001	-28672	-100 – 8000	Blue band aerosol optical depth
Optical_Depth_055	INT16	0.001	-28672	-100 – 8000	Green band aerosol optical depth
AOD_Uncertainty	INT16	0.0001	-28672	0 – 30000	AOD uncertainty
FineModeFraction	FLOAT32	n/a	-99999	0 – 1000	Fine mode fraction over the ocean
Column_WV	INT16	0.001	-28672	0 – 30000	Column Water Vapor (cm)
Injection_Height	FLOAT32	n/a	-99999	0 - 10000	Smoke injection height (m above ground)
AOD_QA	UINT16	n/a	0	1 – 65535	AOD QA
AngstromExp_470-780	INT16	0.0001	-28672	-5000 – 30000	Angstrom Exponent 470-780nm over the ocean
cosSZA	INT16	0.0001	-28672	0 – 10000	Cosine of Solar zenith angle (5km)
cosVZA	INT16	0.0001	-28672	0 – 10000	Cosine of View zenith angle (5km)
RelAZ	INT16	0.01	-28672	-18000 – 18000	Relative azimuth angle (5km)
Scattering_Angle	INT16	0.01	-28672	-18000 – 18000	Scattering Angle (5km)
Glint_Angle	INT16	0.01	-28672	-18000 – 18000	Glint Angle (5km)

5.4 AOD QA definition for MCD19A2 (16-bit unsigned integer)

Bits	Definition
0-2	**Cloud Mask** 000 --- Undefined 001 --- Clear 010 --- Possibly Cloudy (detected by AOD filter) 011 --- Cloudy (detected by cloud mask algorithm) 101 --- Cloud Shadow 110 --- Hot spot of fire 111 --- Water Sediments
3-4	**Land Water Snow/Ice Mask** 00 --- Land 01 --- Water 10 --- Snow 11 --- Ice
5-7	**Adjacency Mask** 000 --- Normal condition/Clear 001 --- Adjacent to clouds 010 --- Surrounded by more than 4 cloudy pixels 011 --- Adjacent to a single cloudy pixel 100 --- Adjacent to snow 101 --- Snow was previously detected in this pixel
8-11	**QA for AOD** 0000 --- Best quality 0001 --- Water Sediments are detected (water) 0011 --- There is 1 neighbor cloud 0100 --- There is >1 neighbor clouds 0101 --- No retrieval (cloudy, or whatever) 0110 --- No retrievals near detected or previously detected snow 0111 --- Climatology AOD: altitude above 3.5km (water) and 4.2km (land) 1000 --- No retrieval due to sun glint (water) 1001 --- Retrieved AOD is very low (<0.05) due to glint (water) 1010 --- AOD within +-2km from the coastline is replaced by nearby AOD 1011 --- Land, research quality: AOD retrieved but CM is possibly cloudy
12	**Glint Mask** 0 --- No glint 1 --- Glint (glint angle < 40°)
13-14	**Aerosol Model** 00 --- Background model (regional) 01 --- Smoke model (regional) 10 --- Dust model
15	**Reserved**

5.5 Daily Gap-Filled Surface Properties (BRDF/NDVI/Snow Properties) (MCD19A3)

SDS name	Data Type	Scale	Fill Value	Valid Range	Description
Kiso	INT16	0.0001	-32767	-32766 – 32767	RTLS isotropic kernel parameter for band 1-8
Kvol	INT16	0.0001	-32767	-32766 – 32767	RTLS volumetric kernel parameter for band 1-8
Kgeo	INT16	0.0001	-32767	-32766 – 32767	RTLS geometric kernel parameter for band 1-8
UpdateDay	UINT8	n/a	255	0 – 254	Number of days since last update to the current day
Snow_Fraction	INT16	0.0001	-28672	0 – 16000	Snow fraction (0-1.6*)
Snow_Grain_Size	INT16	0.001	-28672	0 – 30000	Snow grain diameter (mm)
Snow_Fit	INT16	0.0001	-28672	0 – 30000	Land+Snow linear mixture model RMSE in bands 1,5,7
Snow_UpdateDay	UINT8	n/a	255	0 – 254	Number of days since last update to the current day for snow fraction and snow grain size
NBAR_250m	INT16	0.0001	-28672	-100-16000	Nadir BRDF-Adjusted Reflectance, Bands 1,2
NDVI1km	INT16	0.0001	-28672	0-10000	Daily Normalized Difference Vegetation Index, gap-filled
NDVI_NBAR_UpdateDay	UINT8	n/a	255	0 – 254	Number of days since last update to the current day for NDVI and NBAR

*The Snow Fraction (grain size) is retrieved from the vis-SWIR bands using the linear mixture surface reflectance model combining the land surface BRDF and a theoretical snow reflectance model. The snow roughness and melt-freeze conditions may create crust on the snow surface resulting in glint that is not accounted for in the theoretical model. Thus, the derived and reported Snow Fraction (representing measured reflectance) may take values above 1 at certain conditions and view geometries, although the physical snow fraction cannot exceed 1.

5.6 Daily 0.05° global surface BRF CMG for Land Bands (MCD19A1CMGL)

SDS name	Data Type	Scale	Fill Value	Valid Range	Description
BRF_B0[1-7]	INT16	0.0001	-28672	0 – 16000	Bidirectional Reflectance Factor, Band01-07
BRFn_B0[1-7]	INT16	0.0001	-28672	0 – 16000	Bidirectional Reflectance Factor normalized to 45° SZA and nadir view, Band01-07
NBAR_B0[1-7]	INT16	0.0001	-28672	0 – 16000	Nadir BRDF-Adjusted Reflectance(NBAR),

					normalized to 1:30pm location time sun angle, Band01-07
QA	UINT8	n/a	255	0-3	Quality Assurance Flag
cSZA	INT16	0.0001	-28672	0-10000	Cosine of Solar zenith angle
cVZA	INT16	0.0001	-28672	0 – 10000	Cosine of View zenith angle
Rel_AZI	INT16	0.01	-28672	-18000 – 18000	Relative Azimuth Angle

5.7 Daily 0.05° global surface BRF CMG for Ocean Bands (MCD19A1CMGO)

SDS name	Data Type	Scale	Fill Value	Valid Range	Description
BRF_B[08-12]	INT16	0.0001	-28672	0 – 16000	Bidirectional Reflectance Factor, Band08-12
BRFn_B[08-12]	INT16	0.0001	-28672	0 – 16000	Bidirectional Reflectance Factor normalized to 45° SZA and nadir view, Band08-12
NBAR_B[08-12]	INT16	0.0001	-28672	0 – 16000	Nadir BRDF adjusted Reflectance(NBAR), normalized to 1:30pm location time sun angle, Band08-12
QA	UINT8	n/a	255	0-3	Quality Assurance Flag
cSZA	INT16	0.0001	-28672	0-10000	Cosine of Solar zenith angle
cVZA	INT16	0.0001	-28672	0 – 10000	Cosine of View zenith angle
Rel_AZI	INT16	0.01	-28672	-18000 – 18000	Relative Azimuth Angle

5.8 Daily 0.05° global surface BRF CMG QA definition

Bits	Definition
0	**Coverage**: 0 --- High Coverage 1 --- Low Coverage
1	**AOD Level:** 0 --- Low AOD 1 --- High AOD

5.9 Daily 0.05° global AOD CMG (MCD19A2CMG)

SDS name	Data Type	Scale	Fill Value	Valid Range	Description
AOD_055	INT16	0.001	-28672	0 – 6000	Daily average of AOD for 550nm band
AOD_047	INT16	0.001	-28672	0 – 6000	Daily average of AOD for 470nm band
Sigma_AOD_055	INT16	0.0001	-28672	0 – 30000	Standard deviation/ Uncertainty of daily AOD for 550nm band
ColumnWaterVapor_Terra	INT16	0.001	-28672	0-30000	Daily average of column water vapor for Terra in cm
ColumnWaterVapor_Aqua	INT16	0.001	-28672	0-30000	Daily average of column water vapor for Aqua in cm
CloudFraction	INT16	0.0001	-28672	0-10000	Daily average cloud fraction
Compact_AOD_055	INT16	0.001	n/a	0-6000	AOD record compacted into 1-D array, for 550nm band
OverpassTime	INT16	n/a	n/a	0-1440	Satellite overpass time in corresponding AOD record, minutes since 00:00 of the given day
Line	INT16	n/a	n/a	0-3599	Y coordinate of compacted AOD record
Sample	INT16	n/a	n/a	0-7199	X coordinate of compacted AOD record
Offset_AOD_055	INT32	n/a	n/a	n/a	Offset in compacted AOD record
nAOD	INT16	n/a	n/a	0-100	Number of AOD in compacted AOD record

The CMG AOD file stores the daily-average AOD (at 0.47 and 0.55μm) as well as AOD from all overpass orbits for a given day. Since the individual orbits data are sparse due to clouds (snow), the orbital data are stored in compact way, similar to MOD09 product. In more detail, the compact format is described at the end of this Manual (sec. 10).

5.10 Daily 0.05° global Vegetation Index CMG (MCD19A3CMG)

SDS name	Data Type	Scale	Fill Value	Valid Range	Description
NDVI	INT16	0.0001	-28672	0 – 10000	Daily Normalized Difference Vegetation Index at surface
NDVI_n	INT16	0.0001	-28672	0 – 10000	Daily NDVI normalized to SZA=45° and nadir view
EVI	INT16	0.0001	-28672	0-10000	Daily Enhanced Vegetation Index at surface

EVI_n	INT16	0.0001	-28672	0-10000	Daily EVI normalized to SZA=45° and nadir view
NDVI_gapfill	INT16	0.0001	-28672	0-10000	Gap-filled NDVI

6. Caveats and Known Problems

1. MAIAC LUTs are built assuming pseudo-spherical correction in single scattering which has a reduced accuracy for high sun/view zenith angles. A reduced MAIAC performance is expected at solar zenith angles > 70°.
2. MAIAC may be missing bright salt pans in several world deserts. In such cases, it generates a persistent high AOD resulting in missing surface retrievals.
3. Because of inherent uncertainties of gridding on the coastline, the area of ±1-3 pixels from the coastline may contain frequent artifacts in cloud mask (usually over-detection), AOD (higher values) and surface BRF. Users should exercise caution near the coastline as indicated by QA.QA_AOD.
4. AC over detected snow: as MAIAC does not retrieve AOD over snow, it assumes a low climatology AOD=0.05 globally and 0.02 at high elevations (H>4.2km). Over north-central China, which is often heavily polluted and low AOD assumption can lead to a significant bias, we use AOD averaged over mesoscale area of 150km using reliable AOD retrievals over snow-free pixels. Such approach does improve quality of AC as compared to low-AOD assumption as judged by the reduced boundaries and color artefacts, but it does not account for the aerosol variability inside 150km area.
5. Ice mask is currently unreliable.
6. Consistently miss a particular type of clouds (moderately thin and homogeneous cumulus) over water generating high AOD.

We are working to resolve remaining issues.

7. MAIAC Validation Status

The atmospheric suite of MAIAC C6 products (MCD19A2) has been extensively validated in both regional and global analyses.

Column water vapor: *Martins* et al. (2017; 2018; 2019) showed the accuracy of 10-15% both over South America and over global land, consistent with our validation analysis.

Aerosol Optical Depth: Due to its high spatial resolution (1km) and high accuracy over both dark and bright surfaces, MAIAC AOD is the most extensively studied and validated product by the Air Quality and, recently, by the climate modeling community. Numerous regional and global validation studies show a high quality of MAIAC AOD product generally on par or exceeding performance of the standard operational Dark Target (DT, *Levy et al*. (2013)) and Deep Blue (DB, *Hsu et al*. (2013)) aerosol algorithms (e.g., *Lyapustin et al*., 2018; *Jethva et al*., 2019; *Chawdhary et al*., 2019; *Mhawish et al*., 2019; *Tao et al*., 2019; *Wei et al*., 2020; *Hammer et al*., 2020; *Schutgens et al*., 2020). MAIAC C6 shows a *global* accuracy of 0.05±0.1AOD (or *10%*) for 67% measurements (*Lyapustin et al.*, 2018; *Martins et al*., 2017), minimal dependence on surface brightness and view geometry compared to DB and DT, as well as minimal winter-spring bias

(*Superczynski et al*., 2017) from better snow detection (*Cooper et al*., 2018). *Schutgens et al.*, (2020) emphasized a *"remarkable consistency"* between MAIAC Terra and Aqua AOD, much higher than that from DB and DT, which is a consequence of our MODIS calibration work.

Smoke Plume Injection Height: A validation against MISR MINX and CALLIPSO CALIOP plume heights for the North America fires of 2000-2008 showed an agreement within ~500m in ~60% of matching cases (*Lyapustin et al*., 2020).

MAIAC Surface Reflectance (MCD19A1): Since its introduction in 2011-2012, MAIAC SR product has been used in land science applications, in particular over highly cloudy tropical regions where MAIAC offers more high quality pixels for vegetation trend and change analysis (e.g. *Hilker et al*., 2012; 2014; 2015; 2017; *Guan et al.*, 2015; *Bi et al*., 2015; *Saleska et al*., 2016; *Yang et al*., 2018; *Wu et al*., 2018). In a limited study using seven MODIS tiles over the North and South American continents in 2002, *Chen et al*. (2017) demonstrated an improvement in the MODIS standard LAI/FPAR retrievals when the algorithm used MAIAC SR input instead of MOD09.

Lyapustin et al. (2021) gave the first systematic comparison of MAIAC C6 (MCD19A1) daily surface reflectance (SR) product with standard MODIS SR (MOD09). The two algorithms have different cloud detection, aerosol retrieval and atmospheric correction: MAIAC uses an accurate BRDF-coupled radiative transfer model and MOD09 uses a Lambertian SR model. Four 1200 km tiles in 2018 located in mid-Atlantic USA, Canada, central Amazon, and northeastern China were used to study spectral and seasonal differences, as well as sensitivity to the aerosol optical depth (AOD) variations. The results of this study can be summarized as follows: a) MAIAC provides from 4% to 25% more high-quality retrievals than MOD09 annually; b) While MAIAC-MOD09 agreement in NIR is very good, there is a systematic difference increasing from NIR to Blue, typical of biases of a Lambertian assumption in MOD09 algorithm; c) Over China, MAIAC SR remains stable at wide range of AOD variations, whereas MOD09 SR shows a consistent positive bias increasing with AOD and at shorter wavelengths. The reported results are characteristic of a global performance as the four selected tiles represent most of the global ecosystems, except arid, and of the weather/climate conditions that define performance of the atmospheric correction algorithms.

8. Data ordering (browsing)

8.1. Where to get MAIAC data

The following tools offer options to search the LP DAAC ((**Land Processes Distributed Active Archive Center)** data holdings and provide access to the data:

1) Bulk download:LP DAAC Data Pool (https://lpdaac.usgs.gov/data_access/data_pool) and DAAC2Disk (https://lpdaac.usgs.gov/data_access/daac2disk)
2) Search and browse: USGS EarthExplorer (https://earthexplorer.usgs.gov/) and NASA Earthdata Search (https://search.earthdata.nasa.gov/search)
3) Subset and explore: AppEEARS (https://lpdaacsvc.cr.usgs.gov/appeears/).
4) MODIS Land Global Browse Images
   5-km versions of selected product to enable synoptic quality assessment.
   Link: http://landweb.nascom.nasa.gov/cgi-bin/browse/browse.cgi

Note: USGS EarthExplorer and AppEEARS access to the data follows soon after public release.

9. REFERENCES

Bi J, Knyazikhin Y, Choi S, Park T, Barichivich J, Ciais P, Fu R, Ganguly S, Hall F, Hilker T, Huete A, Jones M, Kimball J, Lyapustin A, Mottus M, Nemani R, Piao S, Poulter B, Saleska S, Saatchi S, Xu L, Zhou L, Myneni R., Sunlight mediated seasonality in canopy structure and photosynthetic activity of Amazonian rainforests, Environ. Res. Lett., 10(6):6, 2015, 10.1088/1748-9326/10/6/064014.

Bi, J., R. Myneni, A. Lyapustin, Y. Wang, T. Park, C. Chen, K. Yan, Y. Knyazikhin, Amazon forests' response to droughts: a perspective from the MAIAC product, Remote Sens., 2016, 8, 356; doi:10.3390/rs8040356.

Chen, C., Y. Knyazikhin, T. Park, K. Yan, A. Lyapustin, Y. Wang, B. Yang and R. B. Myneni, Prototyping of LAI and FPAR Algorithm with MODIS MultiAngle Implementation of Atmospheric Correction (MAIAC) data, Rem. Sensing, 2017, 9, 370; doi:10.3390/rs9040370.

Cooper, M. J., Martin, R. V., Lyapustin, A. I., and McLinden, C. A.: Assessing snow extent data sets over North America to inform and improve trace gas retrievals from solar backscatter, Atmos. Meas. Tech., 11, 2983-2994, doi:10.5194/amt-11-2983-2018, 2018.

Guan, K., Pan, M., Li, H., Wolf, A., Wu, J., Medvigy, D., Caylor, K. K., Sheffield J., Wood, E.F., Malhi, Y., Liang, M., Kimball, J. S., Saleska, S., Berry, J., Joiner, J., and Lyapustin, A. I. (2015) "Photosynthetic seasonality of global tropical forests constrained by hydroclimate", Nature Geoscience, 8, 284-289, doi: 10.1038/NGEO2382.

Hammer, M.S.; van Donkelaar, A.; Li, C.; Lyapustin, A.; Sayer, A.M.; Hsu, N.C.; Levy, R.C.; Garay, M.J.; Kalashnikova, O.V.; Kahn, R.A.; et al. Global Estimates and Long-Term Trends of Fine Particulate Matter Concentrations (1998-2018). Environ. Sci. Technol. 2020, 54, 7879–7890, https://doi.org/10.1021/acs.est.0c01764.

Hilker, T., A. Lyapustin, F. G. Hall, Y. Wang, N. C. Coops, G. Drolet, & T. A. Black, 2009: An assessment of photosynthetic light use efficiency from space: Modeling the atmospheric and directional impacts on PRI reflectance. Rem. Sens. Environment, 113, 2463-2475.

Hilker, T., Hall, F., Coops, N.C., Lyapustin, A., Wang, Y., Nesic, Z., Grant, N., Black, T.A. Wulder, MA., Kljun, N., Hopkinson, C., Chaser, L., 2010: Remote sensing of photosynthetic light-use efficiency across two forested biomes: Spatial scaling. Rem. Sens. Environ., 114, 2863-2874.

Hilker, T., A. I. Lyapustin, C. J. Tucker, P. J. Sellers, F. G. Hall, Y. Wang, 2012: Remote Sensing of Tropical Ecosystems: Atmospheric Correction and Cloud Masking Matter. Rem. Sens. Environ., http://dx.doi.org/10.1016/j.rse.2012.08.035**.**

Hilker, T., A. I. Lyapustin, C. J. Tucker, F. G. Hall, R. B. Myneni, Y. Wang, J. Bi, Y. M. de Moura, P. J. Sellers (2014), Vegetation dynamics and rainfall sensitivity of the Amazon, PNAS, 111 (45), 16041-16046, doi:10.1073/pnas.1404870111.

Hilker, T., A. I. Lyapustin, Y. Wang, F. G. Hall, C. J. Tucker, P. J. Sellers, On the measurability of change in Amazon vegetation from MODIS, Remote Sens. Environ., 166, 233-242, 2015.

Hsu, N.-Y. C., M.-J. Jeong, C. Bettenhausen, et al. A. M. Sayer, R. A. Hansell, C. S. Seftor, J. Huang, and S.-C. Tsay. 2013. "Enhanced Deep Blue aerosol retrieval algorithm: The second generation." J. Geophys. Res. Atmos., 118 (16): 9296–9315 [10.1002/jgrd.50712.

Jethva, H., O. Torres, R.D. Field, A. Lyapustin, R. Gautam, V. Kayetha, Connecting Crop Productivity, Residue Fires, and Air Quality over Northern India, Nature Scientific Reports, 9:16594, 2019, publ. Nov. 2019.

Levy, R. C., Mattoo, S., Munchak, L. A., Remer, L. A., Sayer, A. M., Patadia, F., and Hsu, N. C.: The Collection 6 MODIS aerosol products over land and ocean, Atmos. Meas. Tech., 6, 2989–3034, doi:10.5194/amt-6-2989-2013, 2013.

Lyapustin, A., C. K. Gatebe, R. Kahn, R. Brandt, J. Redemann, P. Russell, M. D. King, C. A. Pedersen, S. Gerland, R. Poudyal, A. Marshak, Y. Wang, C. Schaaf, D. Hall, and A. Kokhanovsky, 2010: Analysis of Snow Bidirectional Reflectance from ARCTAS Spring-2008 Campaign. Atmos. Chem. Phys., 10, 4359-4375.

Lyapustin, A., J. Martonchik, Y. Wang, I. Laszlo, S. Korkin, 2011a: Multi-Angle Implementation of Atmospheric Correction (MAIAC): Part 1. Radiative Transfer Basis and Look-Up Tables, J. Geophys. Res., 116, D03210, doi:10.1029/2010JD014985.

Lyapustin, A., Y. Wang, I. Laszlo, R. Kahn, S. Korkin, L. Remer, R. Levy, and J. S. Reid, 2011b: Multi-Angle Implementation of Atmospheric Correction (MAIAC): Part 2. Aerosol Algorithm, J. Geophys. Res., 116, D03211, doi:10.1029/2010JD014986.

Lyapustin, A., Y. Wang, I. Laszlo, T. Hilker, F. Hall, P. Sellers, J. Tucker, S. Korkin, 2012: Multi-Angle Implementation of Atmospheric Correction for MODIS (MAIAC). 3: Atmospheric Correction. Rem. Sens. Environ. (2012), http://dx.doi.org/10.1016/j.rse.2012.09.002.

Lyapustin, A., Y. Wang, X. Xiong, G. Meister, S. Platnick, R. Levy, B. Franz, S. Korkin, T. Hilker, J. Tucker, F. Hall, P. Sellers, A. Wu, A. Angal (2014), Science Impact of MODIS C5 Calibration Degradation and C6+ Improvements, Atmos. Meas. Tech., 7, 4353-4365, doi:10.5194/amt-7-4353-2014.

Lyapustin, A., Wang, Y., Korkin, S., and Huang, D.: MODIS Collection 6 MAIAC Algorithm, Atmos. Meas. Tech., 11, 5741-5765, https://doi.org/10.5194/amt-11-5741-2018, 2018.

Lyapustin, A. I., Y. Wang, S. Korkin, R. Kahn, D. Winker, MAIAC Thermal Technique for Smoke Injection Height from MODIS, IEEE Geoscience and Remote Sensing Letters, 17 (5), 730-734, 2020, doi: 10.1109/LGRS.2019.2936332.

Lyapustin A., Zhao F. and Wang Y. (2021) A Comparison of Multi-Angle Implementation of Atmospheric Correction and MOD09 Daily Surface Reflectance Products From MODIS. Front. Remote Sens. 2:712093. doi: 10.3389/frsen.2021.712093

Martins, V. S., A. Lyapustin, L. A. S. de Carvalho, C. C. F. Barbosa, and E. M. L. M. Novo (2017), Validation of high-resolution MAIAC aerosol product over South America, J. Geophys. Res. Atmos., 122, doi:10.1002/2016JD026301.

Martins, V.S., E.M.L.M. Novo, A. Lyapustin, L.E.O.C. Aragão, S.R. Freitas, C.C.F. Barbosa, 2018. "Seasonal and interannual assessment of cloud cover and atmospheric constituents across the Amazon (2000–2015): Insights for remote sensing and climate analysis." ISPRS J. Photogrammetry and Rem. Sens., [10.1016/j.isprsjprs.2018.05.013].

Martins, V.S., A. Lyapustin, Y. Wang, D.M. Giles, A. Smirnov, I. Slutsker, and S. Korkin, Global validation of columnar water vapor derived from EOS MODIS-MAIAC algorithm against the ground-based AERONET observations, Atm. Research, 225, Sept. 2019: 181-192. doi:10.1016/j.atmosres.2019.04.005.

Meister, G., B. Franz, E. Kwiatkowska, and C. McClain (2012). Corrections to the Calibration of MODIS Aqua Ocean Color Bands derived from SeaWiFS Data, *IEEE TGARS*, *50*(1), 310 – 319, doi: 10.1109/TGRS.2011.2160552.

Mhawish, A., T. Banerjee, M. Sorek-Hamer, A.I. Lyapustin, D.M. Broday, R. Chatfield, Comparison and evaluation of MODIS Multi-Angle Implementation of Atmos-pheric Correction (MAIAC) aerosol product over South Asia, Remote Sensing of Environment, 224, pp. 12-28, 2019, https://doi.org/10.1016/j.rse.2019.01.033.

Saleska, S. R., Wu, J., Guan, K., Restrepo-Coupe, N., Nobre, A. D., Araujo, A., & Huete, A. R. (2016). Dry-season greening of Amazon forests. Nature Brief Communication Arising, 531(7594), E4–E5. http://dx.doi.org/10.1038/nature16457.

Schutgens, N., A.M. Sayer, A. Heckel, C. Hsu, H. Jethva, G. de Leeuw, P.J.T. Leonard, R.C. Levy, A. Lipponen, A. Lyapustin, P. North, T. Popp, C. Poulson, V. Sawyer, L. Sogacheva, G. Thomas, O. Torres, Y. Wang, S. Kinne, M. Schulz, and P. Stier, An AeroCom/AeroSat study: Intercomparison of Satellite AOD Datasets for Aerosol Model Evaluation, Atmos. Chem. Phys., 20, 12431–12457, Oct. 2020, https://doi.org/10.5194/acp-20-12431-2020.

Superczynski S., S. Kondragunta, A. Lyapustin. Evaluiation of the Multi-Angle Implementation of Atmospheric Correction (MAIAC) Aerosol Algorithm through Intercomparison with VIIRS Aerosol Products and AERONET, J. Geophys. Res.-Atmos., 2017, 122, 3005-3022, doi:10.1002/2016JD025720.

Toller, G., X. Xiong, J. Sun, B. N. Wenny, X. Geng, J. Kuyper, A. Angal, H. Chen, S. Madhavan, and A. Wu, "Terra and Aqua Moderate-resolution Imaging Spectroradiometer Collection 6 Level 1B Algorithm", J. Applied Remote Sensing, 7(1), 2013, 0001;7(1):073557-073557. doi:10.1117/1.JRS.7.073557.

Vermote, E. F., and Kotchenova, S., 2008: Atmospheric correction for the monitoring of land surfaces. J. Geophys. Res., 113, D23S90, doi:10.1029/2007JD009662.

Xiong X, Angal A, Chang T, Chiang K, Lei N, Li Y, Sun J, Twedt K, Wu A. MODIS and VIIRS Calibration and Characterization in Support of Producing Long-Term High-Quality Data Products. Remote Sensing. 2020; 12(19):3167. https://doi.org/10.3390/rs12193167

Wolfe, R. E., Roy, D. P., and Vermote (1998). E. MODIS Land Data Storage, Gridding, and Compositing Methodology: Level 2 Grid. IEEE Trans. Geosci. Remote Sens., 36, 1324–1338.

Wu, J., Kobayashi, H., Stark, S.C., Meng, R., Guan, K., Tran, N.N., Gao, S., Yang, W., Restrepo-Coupe, N., Miura, T., Oliviera, R.C., Rogers, A., Dye, D.G., Nelson, B.W., Serbin, S.P., Huete, A.R., Saleska, S.R. Biological processes dominate seasonality of remotely sensed canopy greenness in an Amazon evergreen forest. New Phytol. 2018. 217, 1507–1520. https://doi.org/10.1111/nph.14939

Yang, J., Tian, H., Pan, S., Chen, G., Zhang, B., Dangal, S. Amazon drought and forest response: Largely reduced forest photosynthesis but slightly increased canopy greenness during the extreme drought of 2015/2016. Glob. Chang. Biol. 2018. 24, 1919-1934. https://doi.org/10.1111/gcb.14056.

We acknowledge the support from MODAPS and MODIS LAADS in accommodating processing and data archive.

10. How to Reconstruct AOD Image from Compact AOD Records

The compact format uses 6 1-D arrays. AOD at 0.55μm is stored line-by-line for all cloud-free pixels sequentially in **Compact_AOD_055**. For a given grid cell, **nAOD** AOD records from all overpasses are stored consecutively, and **Offset_AOD_055** gives an offset for the grid cell in 1-D array. The respective coordinates of the grid cells are stored in layers "Line" and "Sample". Different orbits are specified by the **OverpassTime** in the same way as **Compact_AOD_055.**

To reconstruct AOD image from compact AOD record, one needs the following 1-D arrays:

Compact_AOD_055: the retrieved $AOD_{0.55}$ (from all orbits) recorded in 1-D array consecutively. Grid cells without retrieval are skipped. For instance, if there are 3 AOD retrievals from different overpasses for a cell (0, 0), the first three numbers will be AOD from these orbits.

Line, Sample: the location of the given cell in 0.05° CMG grid. It can be used to calculate the latitude and longitude of the upper-left corner of the grid cell:

Latitude = 90 – Line * 0.05

Longitude = -180 + Sample*0.05

Offset_AOD_055: The offset of the AOD record for a given cell in Compact_AOD_055 array.

nAOD: Number of AOD records of the day for a given grid cell.

OverpassTime: The time (in minute from GMT time 00:00 of the day) of measurement for a given record. It corresponds one-to-one to Compact_AOD_055.

To reconstruct global AOD image from this compacted 1-D AOD array, one needs to

1) create a 3600x7200 empty grid AODImg;
2) find the grid cells with retrievals from Line/Sample array;
3) find the offset location in Compact_AOD_055 from Offset_AOD_055;
4) Find the AOD and overpass time (orbit) for the n-th overpass:

AODImg[Line][Sample] = Compact_AOD_055[offset+n]

TimeImg[Line][Sample] = OverpassTime[offset+n]

Please, make sure index **n** does not exceed nAOD for a given cell.

11. Compositing BRF Selection Strategy: